CONDENSATION HEAT FLUX MEASUREMENTS IN AMBIENT CONDITIONS ON SUPERHYDROPHOBIC NANOSTRUCTURED SURFACES

BY

JESUS ALFREDO SOTELO

THESIS

Submitted in partial fulfillment of the requirements
for the degree of Master of Science in Mechanical Engineering
in the Graduate College of the
University of Illinois at Urbana-Champaign, 2017

Urbana, Illinois

Adviser:

Assistant Professor Nenad Miljkovic

ABSTRACT

Water vapor condensation is a natural phenomenon experienced in everyday life which can be combined with non-wetting surfaces to enhance heat transfer, desalination, anti-icing and self-cleaning. Recently, superhydrophobic coatings have gathered attention with jumping droplets with the potential for self-cleaning applications and spot cooling on high powered applications. With new coatings being used on different materials, a need has developed for heat transfer measurements through these superhydrophobic coatings as typical heat transfer calculations have been known to underestimate the total heat transfer. Here, I propose to measure the heat flux of a superhydrophobic, nanostructured surface without the need for a controlled vacuum environment. By measuring heat flux within an individual droplet and multiple droplets within a surface, we show that it is possible to measure heat flux of a surface without the need for expensive equipment. As a means of validating these results, experiments within a vacuum chamber will be repeated; hence, the author has provided notes regarding the vacuum chamber building process. This work demonstrates the ability for other researchers to know the heat flux density of a newly fabricated surface to perform initial calculations. Further experiments will involve a vacuum chamber in which similar experiments will be run to be able to compare data and see the effect of atmospheric conditions and non-condensable gasses.

ACKNOWLEDGMENTS

I would like to thank the Mechanical Science and Engineering Department at the University of Illinois at Urbana-Champaign for their financial and academic support throughout my graduate degree. To my professors, mentors, and everyone else who took the time to listen, thank you for keeping my head on straight.

To my teacher, research adviser, and friend, Professor Nenad Miljkovic, thank you for giving me the opportunity to work in the Energy Transport Research Lab and for the support and guidance you've given me throughout classes, research, and life. It was a privilege to learn and work alongside with my lab mates and grow as an individual. I would also like to thank Mr. Jorge Anaya, Mr. Adam Castañeda, and Mr. Ramon Mosqueda for their help in building the test facility and the tedious work in collecting data.

Finally, to my wife, Perla, thank you for always supporting me throughout all of my work and in life, you are my anchor and you always keep me in the right path. To my sister, Erika, thank you for everything you've done for me; growing up was not easy for us and I would not be where I am in life if it wasn't for you. To my parents, thank you for taking the leap of faith coming to a new country and for working so hard.

Gracias a todos.

TABLE OF CONTENTS

CHAPTER 1: INTRODUCTION

Condensation is a natural phenomenon observed in everyday life whether it is while enjoying a cold drink on a hot summer day, or within a 2,300 MW nuclear power plant extracting electricity from steam turbines [1-2]. Dropwise condensation, in particular, is a commonly occurring phenomena in nature which is when a vapor condenses on a non-wetting surface; this can be found in plants such as the lotus leaf and on insect wings such as that found on a cicada [3]. In nature, dropwise condensation can lead to jumping droplets which is used as a self-cleaning mechanism thanks to the superhydrophobic nature of a wing, for example. In industry, however, dropwise condensation has been known to increase heat transfer by an order of magnitude by preventing the surface from becoming flooded, also known as film-wise condensation, which can be detrimental to heat transfer [4]. Along with dropwise condensation, self-induced droplet jumping has been known to occur. This droplet jumping is a result of the coalescence of two or more water droplets on ultra-low adhesion surfaces by converting excess surface energy into kinetic energy [5-9]. There has been much interest in jumping droplets on superhydrophobic surfaces due to the heat transfer enhancement with the potential application for electronic spot cooling [10-11].

The wettability of a surface is governed by the Young-Laplace equation which is a function of the specific surface energies between the vapor, liquid, and gas phase and is defined between the liquid-vapor interface and a solid surface as seen in Equation 1,

$$cos\theta = \frac{\sigma_s - \sigma_i}{\sigma} \tag{1}$$

where θ is the equilibrium contact angle which ranges from 0 (completely wetting) to π (completely non-wetting), σ_s is the specific solid-vapor surface energy, σ_i is the specific solid-

liquid surface energy, and σ is the specific liquid-vapor surface energy of a droplet. The equilibrium contact angle, θ, will lie between θ_A and θ_R, the advancing and receding contact angle [12]. A highly conformal coating or smooth surface will have little to no contact angle hysteresis, which is the difference between the advancing and receding contact angle.

Upon nucleation, a water droplet will either exist in the Cassie-Baxter wetting state where the droplet lies completely on top of the structured surface, or the Wenzel wetting state where the droplet partially or totally fills the cavities within the structures [13]. The superhydrophobic samples prepared in the laboratory setting experienced the Wenzel state which explains why water droplets had a tendency to stick to the surface rather than rolling off when impacted by a light horizontal air velocity.

Much of the inspiration to create superhydrophobic surfaces has come from naturally occurring surfaces which have been created with relative success. Now efforts are geared towards a durable surface. To create a superhydrophobic surface, nano-structuring must be done on a clean surface to reduce adhesion of water droplets, then coated with a low surface energy material [11-16]. Silanes make an adequate source for a low energy surface material; in particular, heptadecafluorodecyltrimethoxysilane (HTMS) as the silane source has been shown to produce high contact angles (>150°) [17]. Producing a non-wetting surface has been done rather successfully, but a sufficiently thin and durable coating has yet to be found.

It is important to accurately characterize these non-wetting surfaces which have a potential to be used in a large energy industry. Heat transfer measurements are especially important to be able to calculate efficiency and operation costs. Copper and steam (water) have widely been studied because of their thermal properties leading to a wide use in industry [18]. Currently, inaccuracies have been known to greatly underestimate heat transfer through superhydrophobic surfaces by not

taking into account higher nucleation densities and the presence of non-condensable gasses. Traditionally, heat transfer is measured by placing thermocouples on a substrate surface and knowing the properties of the surrounding environment, therefore calculating the heat flux from the temperature gradient [19- 21]. The presence of non-condensable gasses can greatly reduce the heat transfer measured during condensation, however, it is known that a vapor cross flow can reduce these effects at low temperatures or before substrate outgassing can occur [22-25]. One challenge with measuring heat transfer during dropwise condensation is taking into consideration the nucleation density of individual water droplets, as well as the diameter of each droplet [26]. Small water droplets (< 10 μm) are known to be most important for heat transfer as they do not form a thermal resistance between the substrate and the environment; thanks to current technology, water droplets of this scale can be distinguished using an electron microscope [27].

Current heat transfer measurement methods involve costly materials such as a vacuum chamber to mitigate the effect on non-condensable gasses [28]. In this work, we measure heat transfer through optical measurements of water droplets (Figure 2.1) in atmospheric conditions in the presence of vapor cross flow. Average heat transfer is also calculated from the entire surface of a sample, and by comparing collected data to future results within a vacuum chamber, we aim to show it is possible to correlate heat transfer simply by measuring water droplet growth in atmospheric conditions.

SCOPE OF RESEARCH

The scope of this research limits heat transfer measurements to manual optical measurements (Figure 2.2) involving a water droplet on a computer screen based on the screen resolution. A more robust system of measurement would involve processing through a software such as MATLAB in which an image is processed and individual water droplets can be measured at different time

intervals. This can come with many obstacles such as resolution, errors with droplet detection, and the ability to differentiate between water droplets. As this method of heat transfer measurements is fairly new, this study will use manual measurements of individual water droplets. The intention will be to validate results within a vacuum chamber and eventually develop a water droplet growth measurement software.

CHAPTER 2: HEAT FLUX METHOD

2.1 CuO Fabrication and Coating

Samples were prepared using 99.9% purity multipurpose 110 Copper, 0.83" thick, with a mirror-like finish. Tabs 1" x 1" were cut and thoroughly cleaned by submersing the bare metal into acetone and sonicating for five minutes, removing the native oxide from the surface. The samples were then rinsed with DI water and then submersed in ethanol and sonicated for five minutes, further cleaning any impurities. The samples were then rinsed in DI water and thoroughly dried using clean nitrogen gas. The clean copper samples were quickly submersed into a hot alkaline solution composed of $NaClO_2$, NaOH, $Na_3PO_4*12H_2O$, and DI water (3.75:5:10:100wt. %) held at 90 °C ± 2° for 10 minutes, or until no further oxidation was visible. During the oxidation process, a thin (≈300 nm) Cu_2O layer was formed on the surface that then re-oxidized to form sharp (Figure 2.3), knife-like CuO oxide structures with heights of $h \approx 1$ μm, rendering the samples superhydrophilic.

The CuO covered samples were deposited with (HTMS) using vapor phase deposition. The Cu samples were placed in a large container faced up along with a small vial containing a 1mL HTMS toluene solution (5% V). The large container was covered and sealed with aluminum foil and was placed in an atmospheric oven at an internal temperature of 80 °C for three hours. This baking process allows for the HTMS molecules to evaporate and deposit onto the CuO, creating a highly conformal coating, making the CuO samples superhydrophobic.

2.2 Microscope Procedure

Droplet growth and distribution behavior were studied using a custom built top-view optical light microscopy set-up shown diagrammatically in Figure 2.2, and substantially similar to the one described in Ref. [11]. Samples were horizontally mounted using a thin layer of thermal grease (Omegatherm, Omega, thermal conductivity of 2.2 W/m·K) to a cold stage (Instec, TP104SC-mK2000A) and cooled to the test temperature of Tw = 5 ± 0.5°C, in a laboratory environment having air temperature, Tair = 22 ± 0.5°C, and relative humidity (RH), Φ = 28 ± 1% (Roscid Technologies, RO120). The RH of the laboratory air could vary up to ± 10% over the course of a day. To ensure stable humidity conditions, the ambient condition experiments were conducted in hour-long segments when the laboratory air RH reached 28%, and ended when the RH exceeded 30% or fell below 26%.

A supply of water-saturated N2 was obtained by sparging a temperature controlled stainless-steel water reservoir with dry N2. A reservoir by-pass valve was installed to provide dry N2 to the sample as it was being cooled to the set point temperature at the beginning of each experiment, Tw = 1 ± 0.5°C. Once the stage temperature stabilized to the test temperature, the by-pass valve was closed to initiate the flow of water-saturated N2 to the sample enclosure at a constant flow rate of $Q \approx$ 2.5 L/min for fast flow and 1.5L/min for slow flow, marking the start of the experiment. The humidity (Roscid Technologies, RO120) was recorded throughout the experiment. The supersaturation was controlled by adjusting the water reservoir temperature through which the N2 was sparged. Experiments were run at two vapor conditions: (1) ambient conditions (no supply vapor flow) corresponding to Tair = 22 ± 0.5°C, Tw = 1 ± 0.5°C, relative humidity Φ = 28 ± 1%, supersaturation S = [ΦPsat(Tair)]/Psat(Tw) = 1.02± 0.035, and nucleation density $N \leq$ 2.5 x 109 droplets/m2, and (2) breath figure conditions corresponding to Tair = 35 ± 0.5°C, Tw = 1 ± 0.5°C,

$\Phi \approx 100 \pm 1\%$, $S = 8.56 \pm 0.4$, and $N \geq 1.1$ x 1010. The second condition (breath figure) was chosen due to our availability to check the conditions by blowing through a 0.5" diameter silicone tube on to the sample, and observing identical condensation conditions as the vapor supply case. Exhaled human breath is composed of CO2 and saturated water vapor at ≈ 36°C.

Video recordings were performed at a frame rate of 1000 frames/s with a high speed camera (Phantom, V711, Vision Research) attached to an upright microscope (Eclipse LV100, Nikon) (Figure 2.2). Top view imaging was performed with a 50X (TU Plan Fluor EPI ELWD, Nikon) objective. The 100X lens made it difficult to resolve the difference between the nano-structures and the ~1 μmdroplets. Illumination was supplied by an LED light source (SOLA SM II Light Engine, Lumencor). The LED light source was specifically chosen for its high-intensity and low power consumption (2.5 W), and narrow spectral range (380 - 680 nm), in order to minimize heat generation at the surface due to light absorption and minimize its influence on the droplet growth rates during condensation. Furthermore, by manually reducing the condenser aperture diaphragm opening size and increasing the camera exposure time, we were able to minimize the amount of light energy needed for illumination and hence minimize local heating effects during condensation experiments.

Droplet nucleation and growth were recorded at variable time intervals using the high speed camera). For the 50X lens, the working distance was measured to be 11 ± 0.5 mm. Prior to experimentation, the size per pixel was calibrated by observing a 10 μm diameter deep reactive ion etched pillar sample at full resolution and at 50X magnification. Prior to optical microscopy, the size of the pillars was known and determined with field emission scanning electron microscopy (S-4800, Hitachi), allowing us to back calculate the minimum size per pixel at 0.075 μm/pixel at the 100X magnification, as seen in Equation 2.

When analyzing the data, regions where large droplets that have recently jumped are optimal as it creates a clear patch of exposed CuO in which fresh droplets can nucleate. Once a droplet nucleates, and its shape can be resolved and measured, it is tracked until the diameter is at least 50% larger. Note that once a droplet coalesces with another droplet, measurement ceases as only growth due to convection of the droplet is sought after. To measure the droplet, its center is recorded as a coordinate in terms of pixels, and then the diameter is measured in pixels as well; this process is continued until the droplet jumps or coalesces.

2.3 Heat Transfer Measurement

To determine the a length from a picture, the following pixel-to-meter conversion is used to determine the diameter of the droplet, d

$$d = 0.075\left[\frac{\mu m}{pixel}\right] * \frac{100}{MM} * \Delta P[pixel] \tag{2}$$

where *MM* is the magnification of the microscope (either 50 for 50X, or 100 for 100X etc.), ΔP is the diameter in pixels of the droplet. This is derived from the screen resolution in the lab setting and can be done with any monitor by calibrating a known length under a microscope and calculating the length per pixel.

The volume of a sphere, which the droplet is approximated as:

$$\forall = \frac{\pi}{6} d^3 \tag{3}$$

To determine the volumetric rate of change of droplet growth, we need a change in volume over a change in time:

$$\dot{\forall} = \frac{\Delta \forall}{\Delta t} \tag{4}$$

where

$$\Delta\forall = \frac{\pi}{6}(d_2^3 - d_1^3) \quad (5)$$

and

$$\Delta t = \Delta Frames[frame] * T[\frac{s}{frame}] \quad (6)$$

By calculating $\dot{\forall}$, it is possible to calculate heat flux since the mass flow rate can be calculated as

$$\dot{m} = \dot{\forall} * \rho \quad (7)$$

where ρ is the density of water $1000[\frac{kg}{m^3}]$ at 5℃

and heat transfer rate $\dot{Q}$ can be calculated as

$$\dot{Q} = \dot{m} * h_{fg} \quad (8)$$

Since area is simply

$$A = \pi * \frac{d_i^2}{4} \quad (9)$$

where d_i is either local diameter (l) or the projected diameter (p) of a droplet. The local area is a function of the contact angle θ, which is $164.5° \pm 1°$ for HTMS coated CuO, and it is the area in direct contact between water droplet and samples.

Measurements were taken for individual water droplets under fast cross vapor flow (Figure 2.4) as well as for multiple droplets averaged over an area (Figure 2.5). A similar procedure was done for individual water droplets (Figure 2.6) and multiple water droplets averaged over an area (Figure 2.7) which experienced slow vapor cross flow.

As seen in Figure 2.8, heat flux density starts relatively high (~ 13 kW/m^2) and quickly decays as the water droplet grows. This is expected since the heat transfer through a water droplet is directly proportional to volumetric flow rate and volumetric flow rate is proportional to the diameter of a water droplet cubed. This means that as the water droplet diameter increases the rate of change decreases. The highest heat flux was observed to happen soon after the droplet nucleates; after this initial value, heat transfer quickly decays as the water droplet become a thermal barrier between the environment and the cold substrate. This behavior to similar to film condensation in

that the heat transfer is greatly reduced once there is liquid water in the way of new water droplet nucleation. When taking measurements as an average of multiple water droplets over an area, we also see a decay in heat flux density, as seen in Figure 2.9. Within Figure 2.8 and 2.9, we see that the initial heat flux density (~ 13 kW/m^2) are within 15% agreement showing that measuring one droplet on a substrate has the possibility of rendering heat flux density of an entire area. A similar argument can be made using data recorded from the slow flow individual and multiple water droplets. Figure 2.10 shows the similar behavior of a high heat flux density (~5 kW/m^2) and quickly decaying to a steady figure. Again, corresponding data can be seen in Figure 2.11 which emphasizes the initial heat flux density of multiple water droplets averaged over an area. It is clear from the data that heat flux density is reduced by at least a factor of two when reducing the speed of the vapor cross flow. This is expected at the heat transfer coefficient of forced convection is reduced for slower flow rates.

2.4 Figures

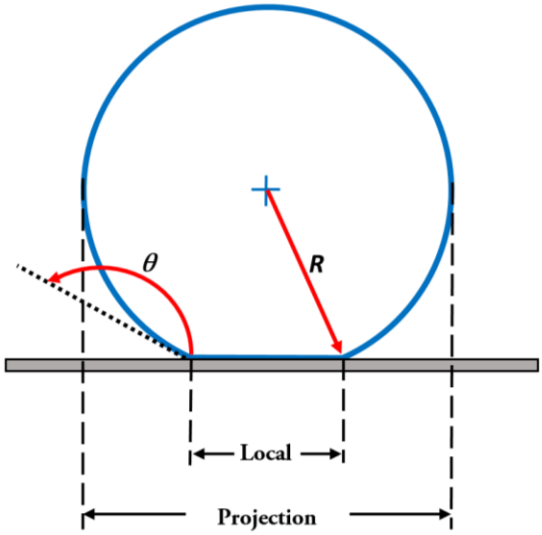

Figure 2.1: Schematic of a single water droplet where the local length represents the local diameter which describes the area in direct contact between the substrate and the water droplet. The projection length is described as the projected area of a water droplet as seen from a top view and is used to calculate the average heat flux density through a single water droplet in [W/m^2].

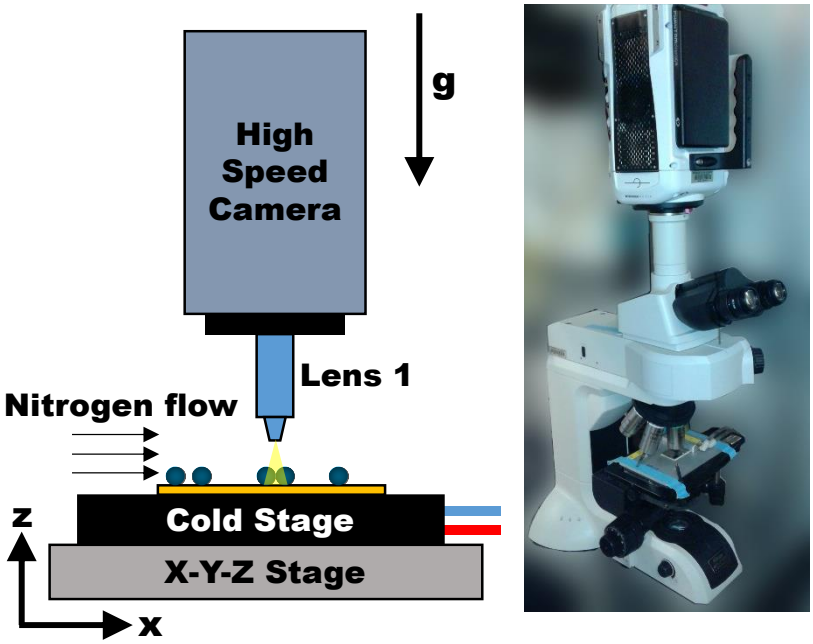

Figure 2.2: Schematic (left) of the top-view experimental setup for droplet measurement. A heated reservoir was used to supply cross flow water vapor to reduce the effects of non-condensable gasses and to provide a constant water vapor source for droplets to condense. Schematic not to scale.

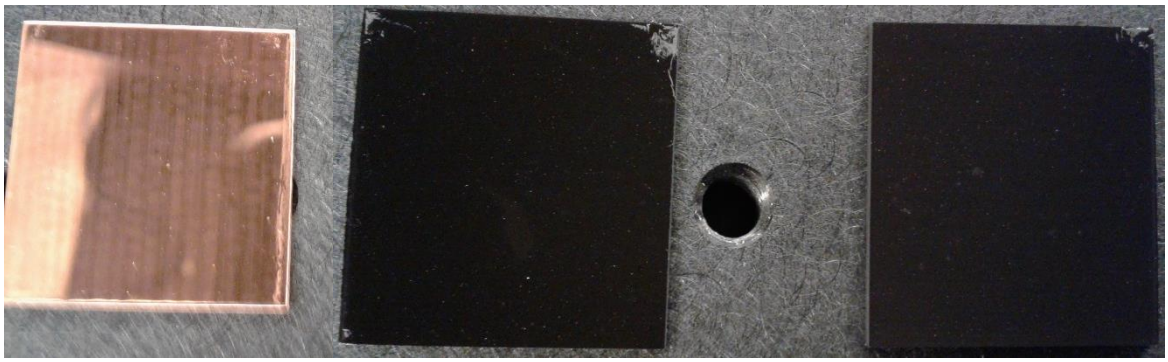

Figure 2.3: From left to right, polished copper before any cleaning, superhydrophilic CuO covered sampled which shows a dark uniform surface containing nano-structures, and a superhydrophobic sample coated with HTMS with a slightly more dull appearance.

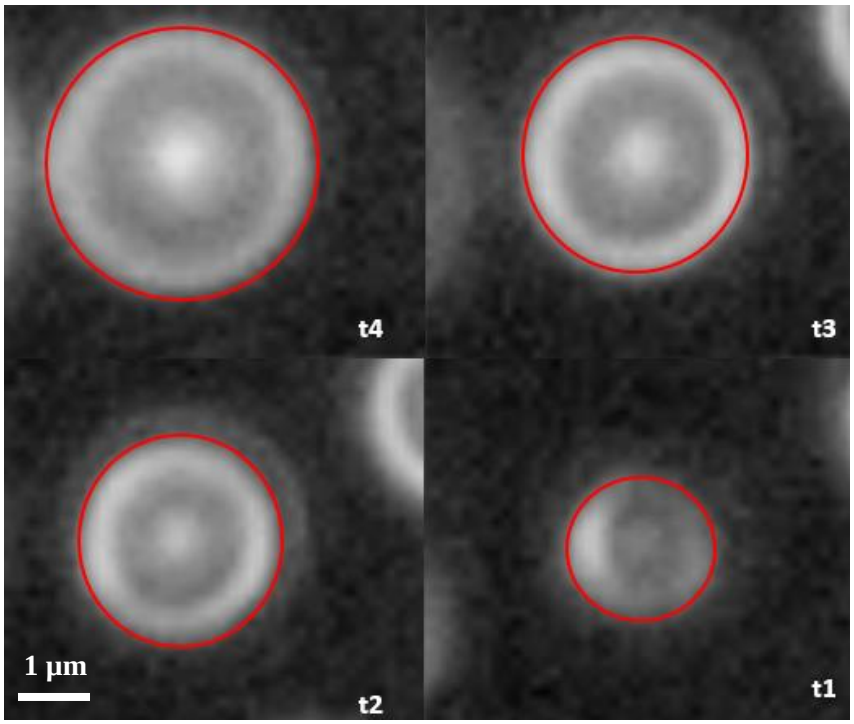

Figure 2.4: Tracking the growth of a single water droplet under fast vapor cross flow at t1= 0 ms, t2 = 164 ms, t3= 393 ms, and t4= 793 ms. It is important to differentiate the difference between the actual water droplet and light diffraction as highlighted in red.

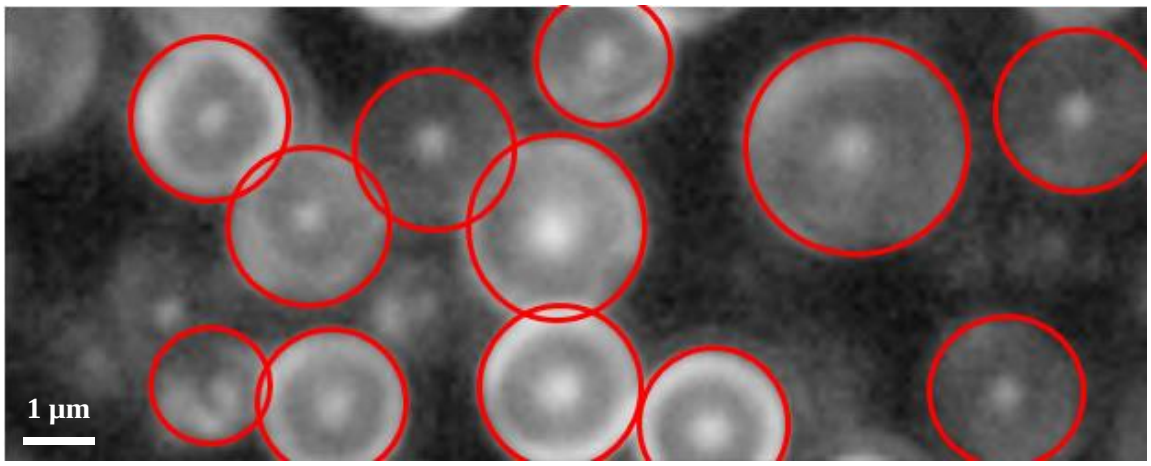

Figure 2.5: Image of multiple droplets experiencing a fast vapor cross flow in a total area of 75 µm^2. Note this is a single point in time; each droplet was measured during multiple time points. If more than 50% of a droplet is within the framed area, then it is counted towards the total average heat flux density.

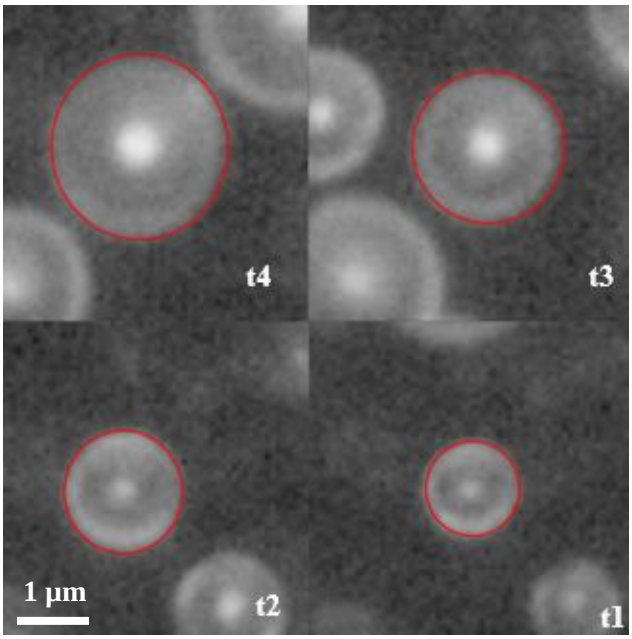

Figure 2.6: Tracking the growth of a single water droplet under slow vapor cross flow at t1= 0 ms, t2 = 1019 ms, t3= 2519 ms, and t4= 5019 ms. It is important to differentiate the difference between the actual water droplet and light diffraction as highlighted in red. It is also important to note how much longer it takes for a droplet to condense.

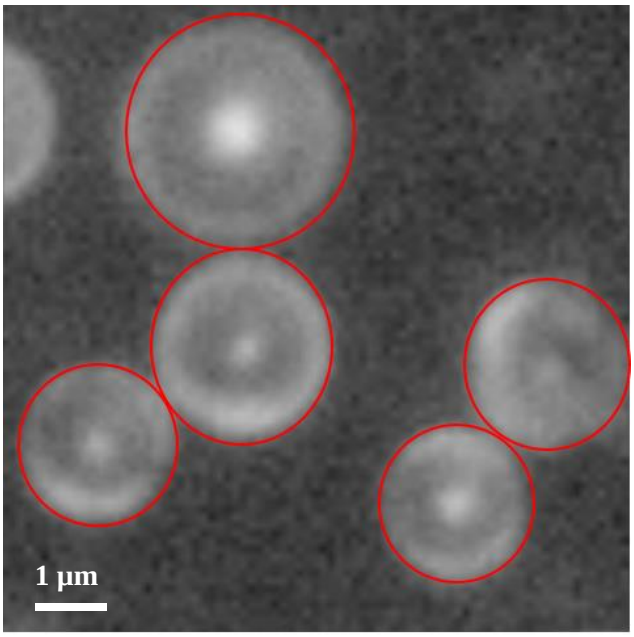

Figure 2.7: Screen shot of multiple droplets experiencing a slow vapor cross flow in a total area of 36 µm^2. Note this is a single point in time; each droplet was measured during multiple time points. If more than 50% of a droplet is within the framed area, then it is counted towards the total average heat flux density.

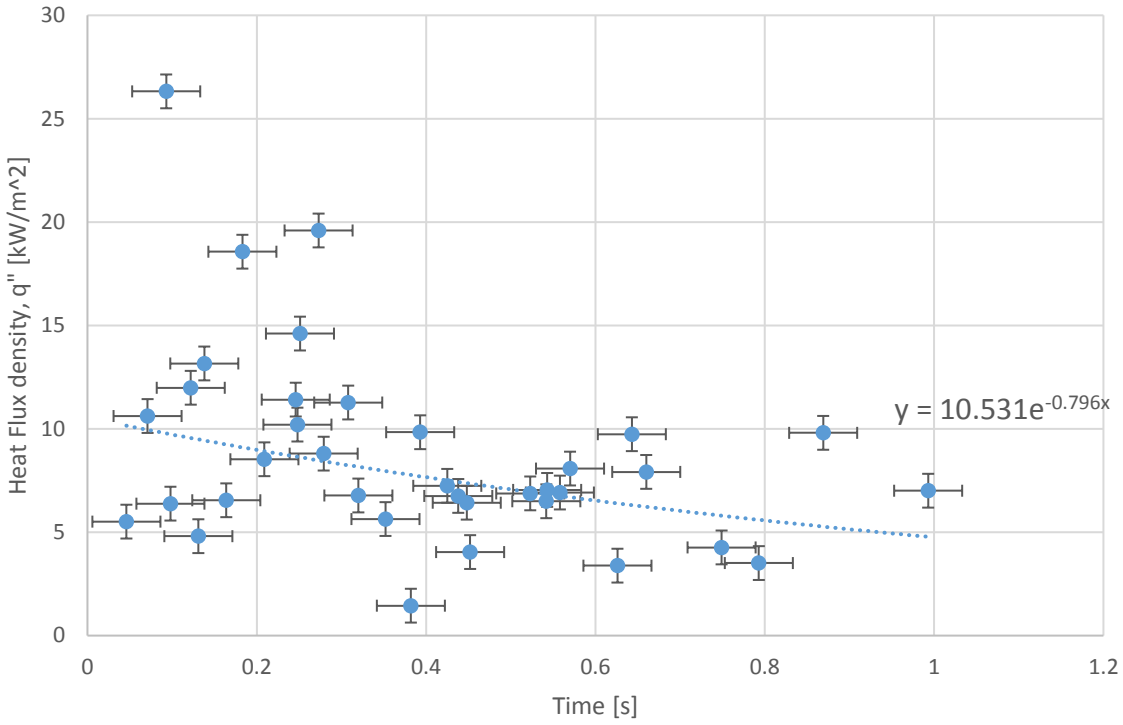

Figure 2.8: Projected heated flux density vs time for single water droplets undergoing fast forced convection. Figure includes standard error bars with an exponential fit trend line.

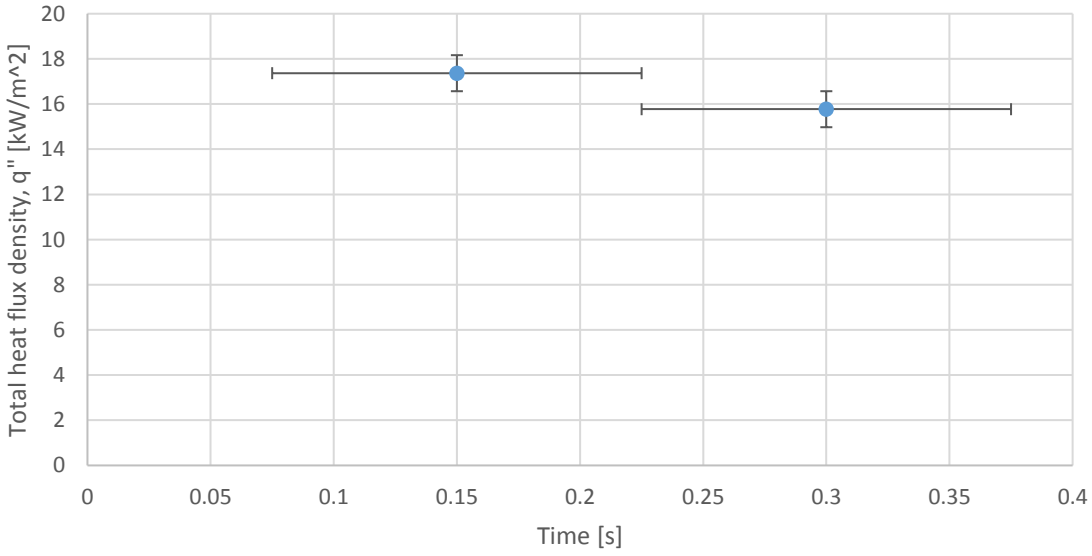

Figure 2.9: Projected heated flux vs time for 20 water droplets undergoing fast forced convection. The area through which the total measured heat transfer occurred was measured as 75 μm^2. Figure includes standard error bars.

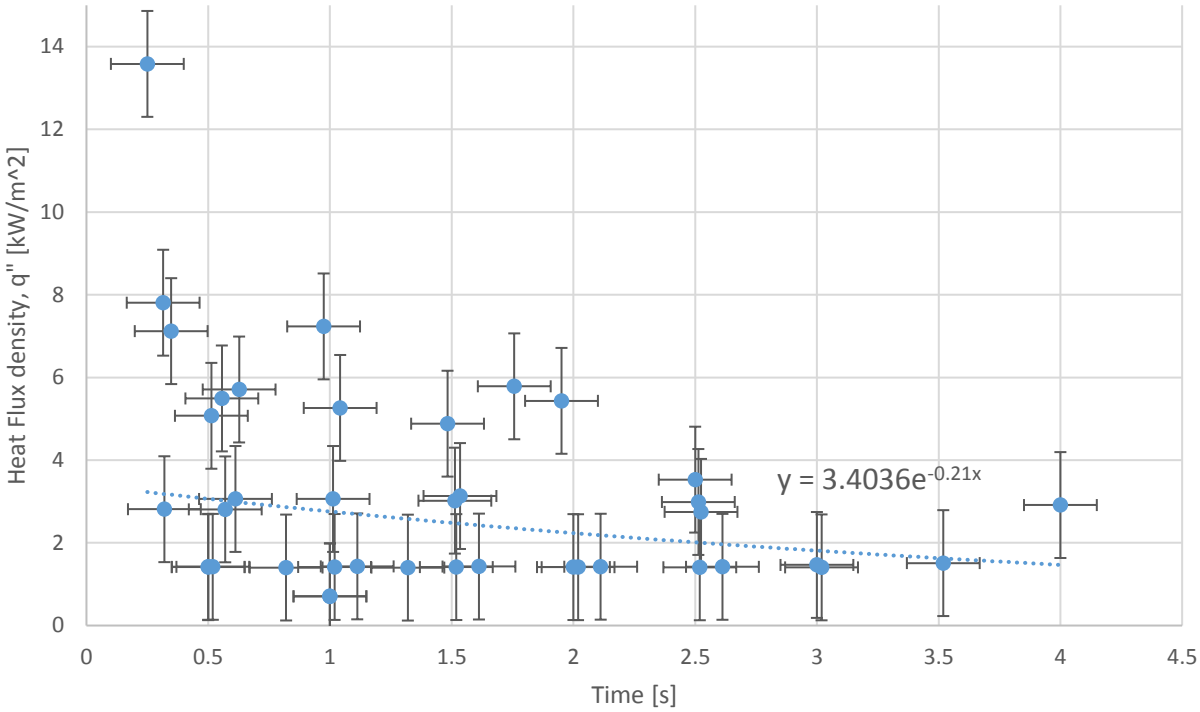

Figure 2.10: Projected heated flux density vs time for single water droplets undergoing slow forced convection. Figure includes standard error bars with an exponential fit trend line.

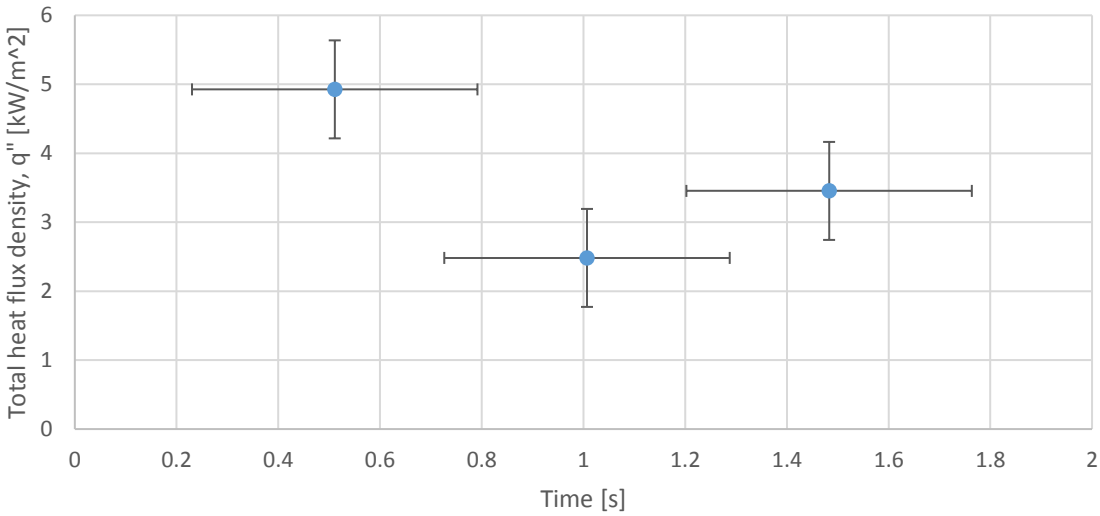

Figure 2.11: Projected heated flux vs time for 20 water droplets undergoing fast forced convection. The area through which the total measured heat transfer occurred was measured as 75 μm^2. Figure includes standard error bars.

CHAPTER 3: VACUUM CHAMBER

3.1 Design Criteria

Validating heat transfer measurement results requires comparisons to values measured within a controlled vacuum chamber environment. To produce a robust and versatile vacuum chamber, one must consider thermocouples, pressure transducer, power feedthroughs and instrumentation feedthroughs, liquid feedthroughs, vacuum level requirements, insulation, optics, and data collection, many of which can be seen in Figure 3.1. Here, I touch on the basic requirements and key points to look out when building a vacuum chamber. Details of vacuum chamber geometry and components can be found in the Appendix A: Vacuum Chamber Schematic section.

3.2 Steam Supply

Ambient conditions in the laboratory setting are 23 °C at 50% relative humidity, at most. The vacuum chamber allows for 100% saturation conditions to promote high water droplet nucleation rates and observe higher heat flux values. To supply steam, an economical and robust vessel was custom ordered from Kurt J. Lesker and manually controlled to produce steam. A 10” full nipple and two 10” CF flanged caps were ordered. One of the caps was used as is on the bottom of the full nipple and one cap was modified by welding five 0.25” tubes through it as seen in Figure 3.2. There were four 6” tubes which were used for a pressure relief valve, steam outlet line, thermocouple probe, and fill line, the 19” probe was used to connect a liquid return line which will be needed for extended experiments. The steam supply vessel can then be filled with deionized water and heated between 80 °C and 100 °C. Heating is provided by four 624 W tape heaters, purchased from ETS Equipment Company, wrapped around the cylindrical vessel in a helical manner, wired in parallel (two sets of two heating tapes were made). Temperature was controlled

using a commercially available 1500 W light dimmer calibrated manually to heat the water in less than 45 minutes. It is important to note that the pressure relief valve should have a line at the outlet leading steam directly to the floor in the event of accidental activation. It was noted that the use of four heating tapes was excessive for the application and one can duplicate a similar system using three 624 W tape heaters using a single 2000 W light dimmer. To reduce heat losses to the environment, and to keep local space at a lower temperature, 2" flexible ceramic blanket insulation was used to cover the steam vessel. Since the vessel in completely sealed, it can be difficult to know how much water there is within. I placed three surface mounted thermocouples on the exterior wall of the steam vessel, being careful not to put it in contact with the tape heaters. Strategically placed in the lower ¾ of the length of the full nipple, one can monitor the temperature of the external thermocouples and observe when the temperature spikes well above water boiling temperature. As the water level decreases within the vessel, the stainless steel can no longer dissipate heat fast enough resulting in localized overheating. Temperatures read from the surface mounted thermocouples can be compared to the 18" thermocouple probe which runs to nearly the bottom of the vessel, which is in direct contact with the deionized water. By comparing data from all four thermocouples, one can have a general idea of when it is time to refill the steam vessel with more deionized water.

3.3 Heaters

The wall temperature for the vacuum chamber was limited by the maximum working temperature of the MKS Micropirani 925 pressure transducer, which was 40 °C. This coincides with a water vapor pressure P_v of 55 Torr, which is quite high for condensation experiments. Since the pressure transducer was placed on the top wall of the vacuum chamber, external heaters were placed on the left, back, and right chamber walls only, to keep the top wall as cool as possible while adequately

heating up the entire chamber. In a similar manner as the steam supply vessel, two 24", 312 W heaters were externally adhered directly onto each of the chamber walls using high temperature polyimide tape and were found to provide adequate heating at 30% capacity. Heaters were wired in parallel and were adjusted using 1500 W light dimmers. This was an initial setup done quickly for the sake of time; if one were to create a more robust setup, there could be a variac to control voltage being sent to the heating tapes and active feedback to a computer software to control chamber wall temperature as well as the steam supply temperature. Heating the walls is important so that condensation does not build up and drip from the top wall and to keep viewports clear of any water droplets. Chamber wall heaters should be left on continuously if experiments will run on a day to day basis since it the walls need to be heated at a low temperature gradient for ~7 hours so that the insulation is not affected. Heating should be done slowly to prevent damage if low temperature insulation is used for the chamber walls. This will also ensure a uniform wall temperature within the chamber walls.

3.4 Viewports

The vacuum chamber has two 8" CF flange viewports (used for visualization and video recording) located on the left side and two 4.5" CF flange viewports on the right side, used for lighting purposes. A cost-benefit analysis was done to decide the flange sizes; an 8" viewport is sufficient for visualizing condensation, but it is recommended to also get an 8" viewport for lighting since high-speed camera applications require a large amount of light. During initial experiments, it was noticed that condensation would form on the viewport glass once steam was introduced into the chamber which was under 15 mTorr vacuum. As mentioned, an optimization must be made between keeping the chambers walls warm without overheating the pressure transducer. A way to circumvent this problem is to create localized heating around the viewport by wrapping a low

power heating tape around the 8” CF flange. One would only need to keep the glass at approximately 50 °C to ensure no condensation formation considering the vacuum levels in which experiments will be done.

3.5 Figures

Figure 3.1: A 24”x24”x24” vacuum chamber purchased from Kurt J Lesker. Pressure, temperature, and image recording capabilities will provide required data to validate results. Vacuum pump setup can reach 1 mTorr which greatly reduces the effects of non-condensable gasses. In clockwise order: a) optical light source, b) high speed camera, c) LN2 trap, d) vent valve, e) vacuum pump, f) type K thermocouple, g) pressure transducer, and h) back lighting source. Note: See Apendix for full chamber schematic and port information.

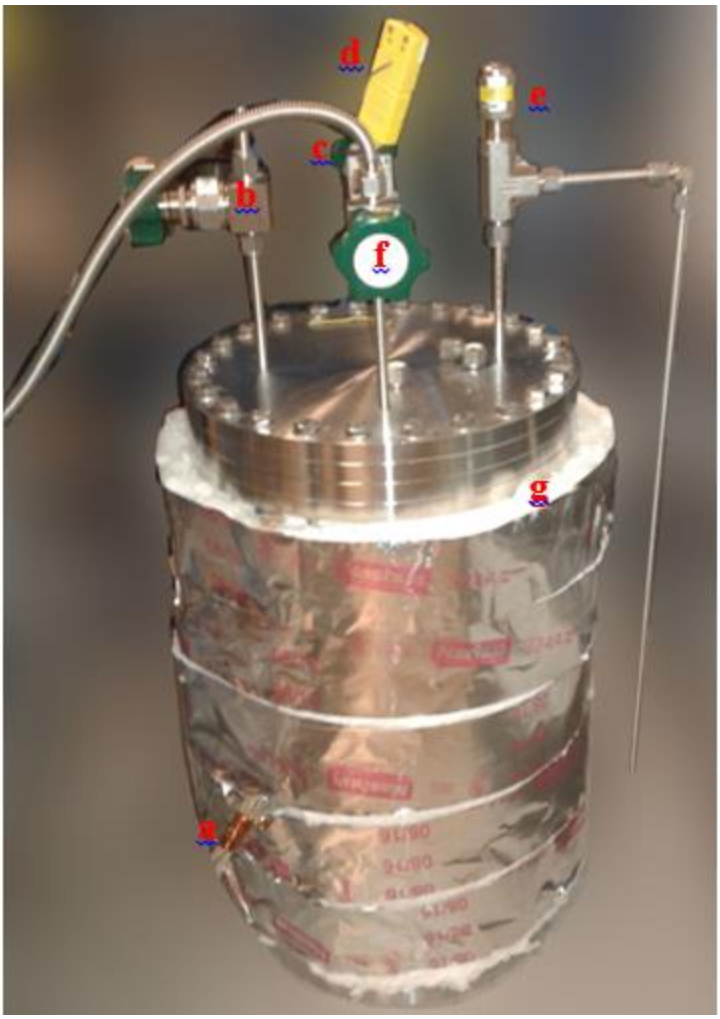

Figure 3.2: Steam supply vessel to introduce 100% saturated water vapor into the vacuum chamber consisting of a 10" CF blank, a 10" full nipple, and a 10" customized blank with five 0.25" tubes welded into it. In clockwise order: a) surface mounted thermocouples which can be used to gauge the water level within the tank, b) a fill line connected with a diaphragm valve, c) extra fill tube for future work involving a liquid return line, d) 18" long thermocouple probe to measure the temperature of the water, e) safety release valve, f) steam supply line leading to vacuum chamber, and g) 2" thick ceramic fiber insulation.

CHAPTER 4: CONCLUSIONS

It is shown that measuring heat flux density through optical microscopy is possible and can be done manually in ambient conditions without the need for expensive equipment, such as a vacuum chamber. Water vapor condensation on a CuO surface coated with HTMS was observed under an electron microscope and heat flux density was calculated from the measured diameter of a water droplet for both individual water droplets as well as multiple water droplets averaged over an area. The measured heat flux density of a single water droplet was in a similar order of magnitude when compared to multiple droplets averaged over an area. This data suggests that heat transfer behavior of a surface can be characterized by optically measuring water droplet growth due to condensation. Future work will involve similar measurements inside of a vacuum chamber which will greatly reduce the effects of non-condensable gasses. Comparing heat flux measurements between ambient conditions and within the chamber will validate results of this work.

REFERENCES

[1] http://www.exeloncorp.com/locations/power-plants/byron-generating-station

[2] L. Perez-Lombard, J. Ortiz, C. Pout, Energ Buildings 2008, 40, 394

[3] Wisdom, Katrina M. et al. "Self-Cleaning of Superhydrophobic Surfaces by Self-Propelled Jumping Condensate." PNAS, 110.20 (2013): 7992–7997. PMC. Web. 7 Apr. 2016

[4] Miljkovic, N.; Wang, E. N. Condensation heat transfer on superhydrophobic surfaces. *Mrs Bull* **2013,** *38* (5), 397-406.

[5] Wilkins, D. G. and Bromley, L. A. (1973), Dropwise condensation phenomena. AIChE J., 19: 839–845. doi:10.1002/aic.690190424

[6] Enright, R.; Miljkovic, N.; Sprittles, J.; Nolan, K.; Mitchell, R.; Wang, E. N. How Coalescing Droplets Jump. *ACS Nano* **2014,** *8* (10), 10352-10362.

[7] Ryan Enright, Nenad Miljkovic, Jorge L. Alvarado, Kwang Kim & John W. Rose (2014) Dropwise Condensation on Micro- and Nanostructured Surfaces, Nanoscale and Microscale Thermophysical Engineering, 18:3, 223-250, DOI: 10.1080/15567265.2013.862889

[8] Miljkovic, N.; Enright, R.; Nam, Y.; Lopez, K.; Dou, N.; Sack, J.; Wang, E. N. Jumping-Droplet-Enhanced Condensation on Scalable Superhydrophobic Nanostructured Surfaces. Nano Letters 2013, 13 (1), 179-187.

[9] Boreyko, J. B.; Chen, C. H. Self-Propelled Dropwise Condensate on Superhydrophobic Surfaces. *Phys Rev Lett* 2009**,** *103* (18), 184501.

[10] J. Oh, P. Birbarah, T. Foulkes, S.L Yin, M. Rentauskas, J. Neely, R.C.N. Pilawa-Podgurski, N. Miljkovic, "Jumping-Droplet Electronics Hot-Spot Cooling," Physics Review Letter, accepted for publication

[11] M. Kim, H. Cha, P. Birbarah, S. Chavan, C. Zhong, Y. Xu, and N. Miljkovic, *Langmuir*, 2015 *31* (49), 13452-13466

[12] Kashchiev, Dimo. "3,5,9,11." *Nucleation: Basic Theory with Applications*. N.p.: Butterworth-Heinemann, 2000. 30+. Print

[13] Aritra Ghosh, Sara Beaini, Bong June Zhang, Ranjan Ganguly, and Constantine M. Megaridis, Enhancing Dropwise Condensation through Bioinspired Wettability Patterning, *Langmuir*, 2014, 30 (43), pp 13103–13115

[14] Enright R, Miljkovic N, Dou N, Nam Y, Wang EN. Condensation on Superhydrophobic Copper Oxide Nanostructures. ASME. *J. Heat Transfer*. 2013;135(9):091304-091304-12. doi:10.1115/1.4024424

[15] Miljkovic, N.; Enright, R.; Wang, E. N. Effect of Droplet Morphology on Growth Dynamics and Heat Transfer during Condensation on Superhydrophobic Nanostructured Surfaces. *Acs Nano* **2012,** *6* (2), 1776–1785.

[16] Miljkovic, N.; Enright, R.; Wang, E. N. Modeling and Optimization of Condensation Heat Transfer on Micro and Nanostructured Superhydrophobic Surfaces. J Heat Transf 2013, doi: 10.1115/1.4024597.

[17] Yang Zhou, A simple way to fabricate an aluminum sheet with superhydrophobic and self-cleaning properties, Chin. Phys. B Vol. 21, No. 12 (2012) 126801

[18] Le Fevre, E. J.; Rose, J. W. Heat-Transfer Measurements During Dropwise Condensation of Steam. International Journal of Heat and Mass Transfer 1964, 7, 272-273.

[19] Ichiro Tanasawa, Advances in Condensation Heat Transfer, Advances in Heat Transfer, Volume 21, 1991, Pages 55-139

[20] S. Necmi, J.W. Rose, Heat-transfer measurements during dropwise condensation of mercury, International Journal of Heat and Mass Transfer, Volume 20, Issue 8, 1977, Pages 877-881

[21] Gagan Deep Bansal , Sameer Khandekar & K. Muralidhar, Measurement of Heat Transfer During Drop-Wise Condensation of Water on Polyethylene, Nanoscale and Microscale Thermophysical Engineering, (2009), 13:3, 184-201, DOI: 10.1080/15567260903077751

[22] E. Citakoglu, J.W. Rose, Dropwise condensation—some factors influencing the validity of heat-transfer measurements, International Journal of Heat and Mass Transfer, Volume 11, Issue 3, 1968, Pages 523-537

[23] E.J. Le Fevre, J.W. Rose, An experimental study of heat transfer by dropwise condensation, International Journal of Heat and Mass Transfer, Volume 8, Issue 8, 1965, Pages 1117-1133

[24] Detlev G. Kroger, Warren M. Rohsenow, Condensation heat transfer in the presence of a non-condensable gas, International Journal of Heat and Mass Transfer, Volume 11, Issue 1, 1968, Pages 15-26

[25] D.W. Tanner, D. Pope, C.J. Potter, D. West, Heat transfer in dropwise condensation at low steam pressures in the absence and presence of non-condensable gas, International Journal of Heat and Mass Transfer, Volume 11, Issue 2, 1968, Pages 181-190

[26] Clark Graham, Peter Griffith, Drop size distributions and heat transfer in dropwise condensation, International Journal of Heat and Mass Transfer, Volume 16, Issue 2, 1973, Pages 337-346

[27] C. Dietz, K. Rykaczewski, A. G. Fedorov, and Y. Joshi, Visualization of droplet departure on a superhydrophobic surface and implications to heat transfer enhancement during dropwise condensation, Applied Physics Letters 97, 033104 (2010); doi: 10.1063/1.3460275

[28] Boreyko, J. B.; Chen, C. H. Vapor chambers with jumping-drop liquid return from superhydrophobic condensers. *International Journal of Heat and Mass Transfer* **2013,** *61*, 409-418.

APPENDIX A: VACUUM CHAMBER SCHEMATIC

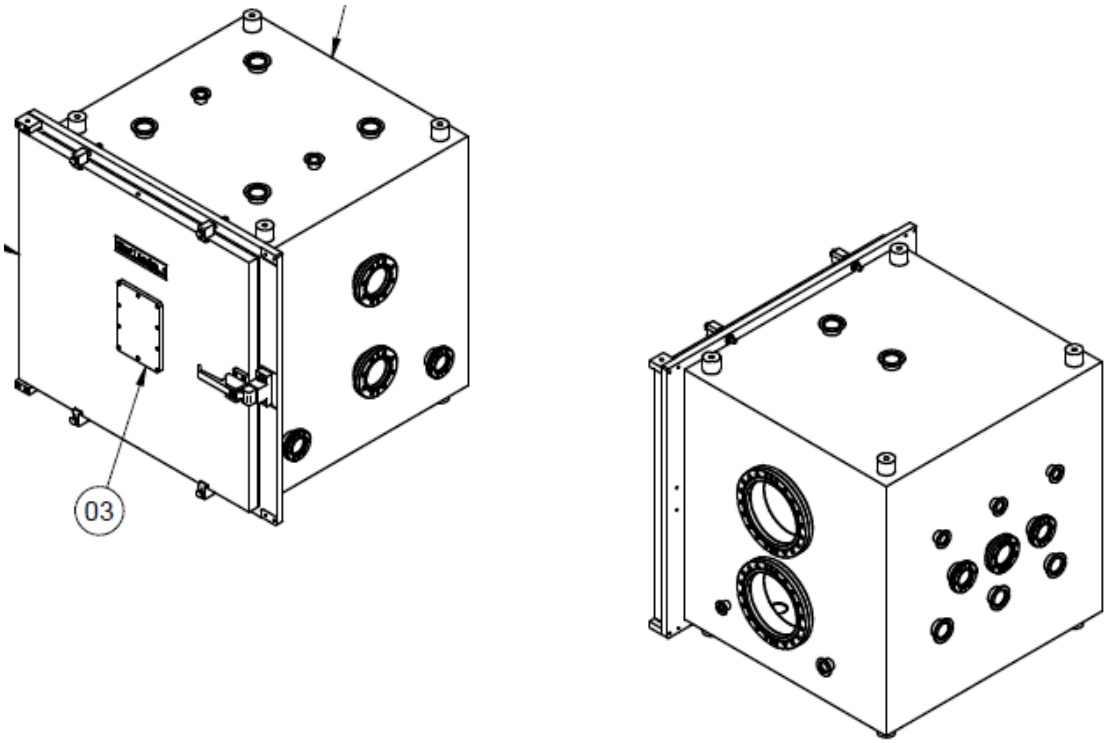

Figure A1: Isometric view of vacuum chamber schematic.

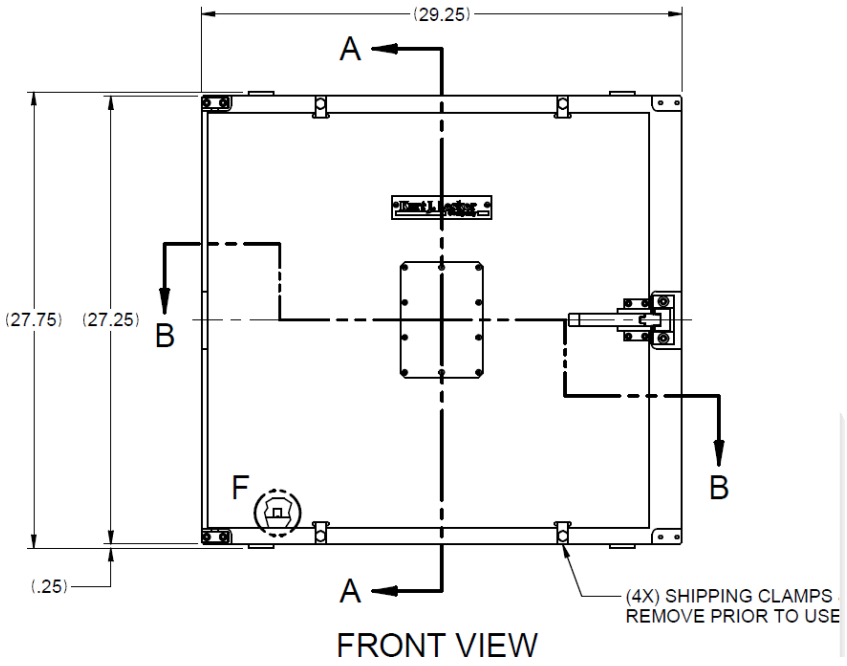

Figure A2: Front view of vacuum chamber including a square viewport.

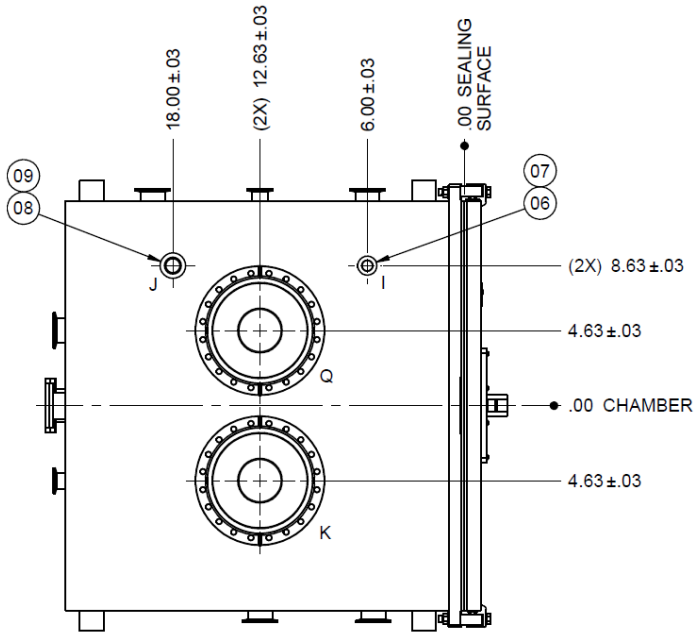

LEFT SIDE VIEW

Figure A3: Left view of vacuum chamber with two 8” CF flanged viewports.

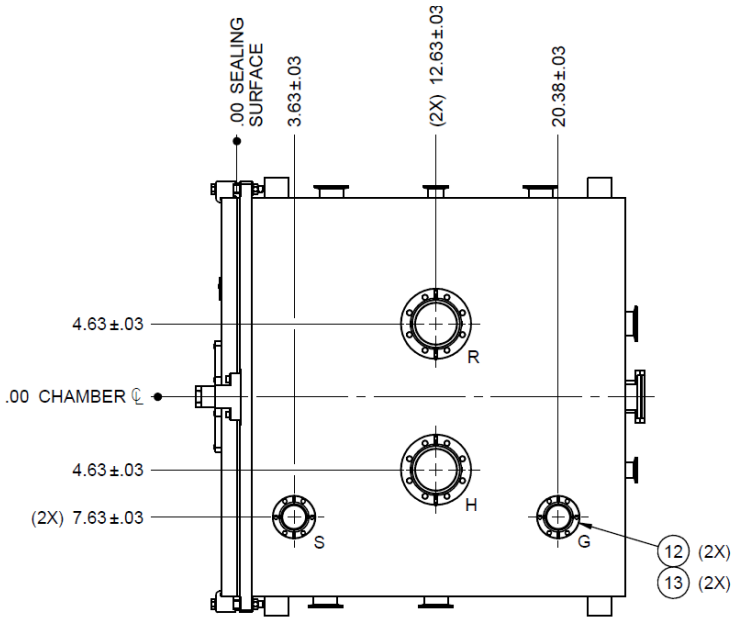

RIGHT SIDE VIEW

Figure A4: Right view of vacuum chamber with two 4.5” CF flanged viewports and two 2.75” CF flanged fluid feedthroughs.

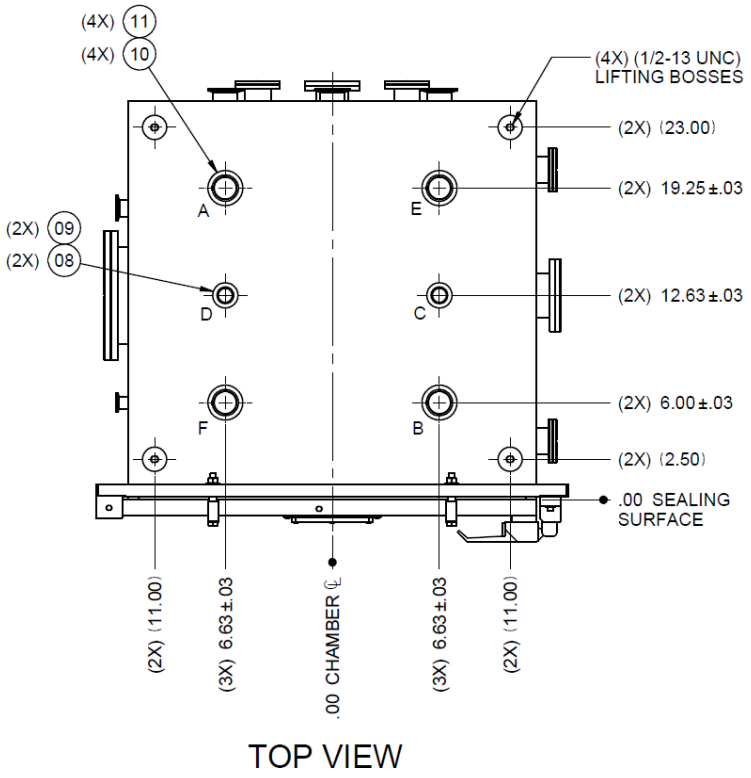

Figure A5: Top view of vacuum chamber with four KF 40 flanges for thermocouples and electrical feedthroughs and two KF 25 flanges for pressure transducer and valve.

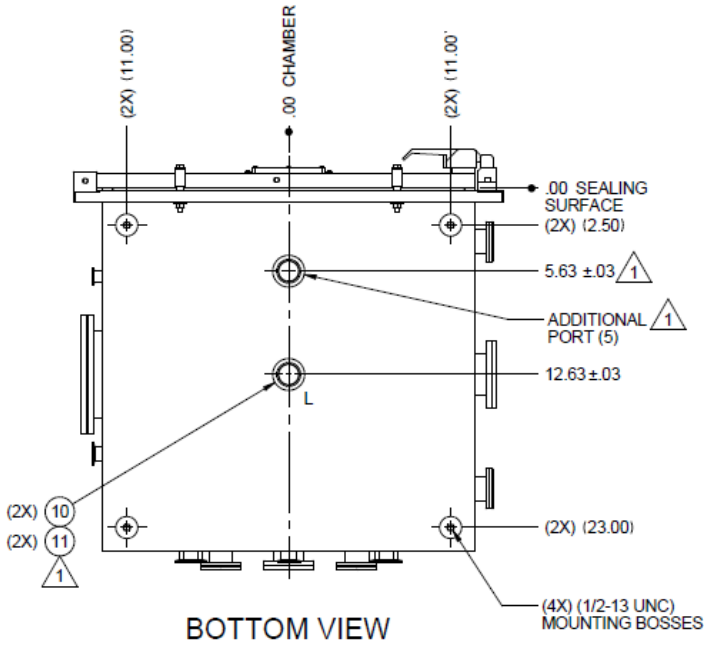

Figure A6: Bottom view of vacuum chamber with two KF 40 flanges for liquid water return.

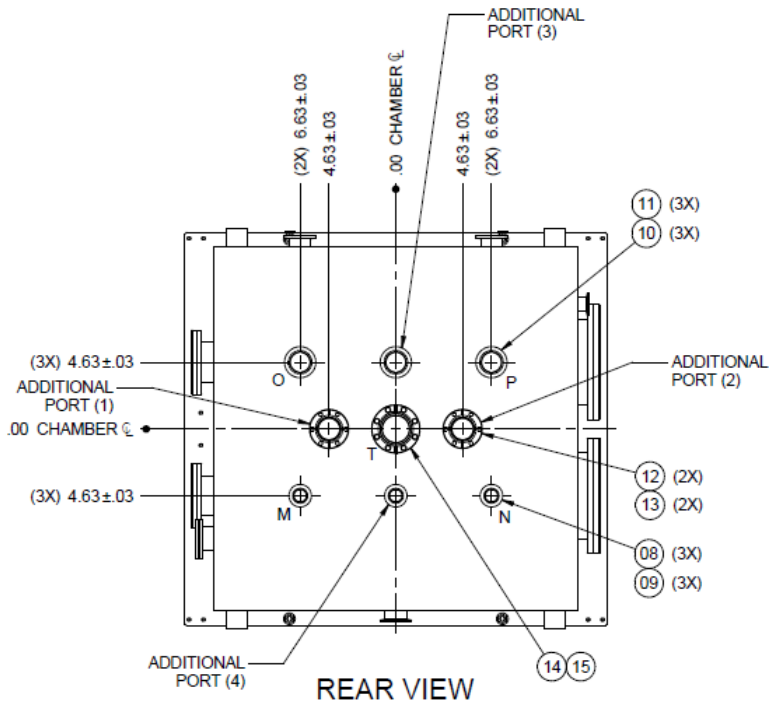

Figure A7: Rear view of vacuum chamber with three KF 40 flanges, three KF 25 flanges, two 2.75” CF flanges and a 3.375” CF flange. Many of these flanges will not be used as they we installed for versatility.